Threshold analysis and biodistribution of fluorescently labeled bevacizumab in human breast cancer

Maximilian Koch[1,2], Johannes S. de Jong[10], Jürgen Glatz[1,2], Panagiotis Symvoulidis[1,2], Laetitia E. Lamberts[4], Arthur L.L. Adams[11], Mariëtte E.G. Kranendonk[10], Anton G.T. Terwisscha van Scheltinga[4,5], Michaela Aichler[3], Liesbeth Jansen[6], Jakob de Vries[6], Marjolijn N. Lub-de Hooge[5], Carolien P. Schröder[4], Annelies Jorritsma- Smit[5], Matthijs D. Linssen[5], Esther de Boer[6], Bert van der Vegt[7], Wouter B. Nagengast[8], Sjoerd G. Elias[12], Sabrina Oliveira[13], Arjen J. Witkamp[14], Willem P.Th.M. Mali[11], Elsken Van der Wall[15], P. Beatriz Garcia-Allende[1,2], Paul J. van Diest[10], Elisabeth G.E. de Vries[4], Axel Walch[3], Gooitzen M. van Dam[6,9] and Vasilis Ntziachristos[1,2]*

Affiliations:

[1]Chair for Biological Imaging, Technical University of Munich, [2]Institute for Biological and Medical Imaging, [3]Research Unit Analytical Pathology, Helmholtz Zentrum, München, Germany

[4]Department of Medical Oncology, [5]Hospital and Clinical Pharmacy, [6]Department of Surgery, [7]Department of Pathology, [8]Department of Gastroenterology, [9]Department of Nuclear Medicine and Molecular Imaging and Intensive Care, University of Groningen, University Medical Center Groningen, the Netherlands

[10]Department of Pathology, [11]Department of Radiology, [12]Julius Center for Health Sciences and Primary Care, Cell Biology,[13]Department of Biology, [14]Department of Surgery, [15]Department of Medical Oncology, Utrecht University, University Medical Center Utrecht, the Netherlands

*Corresponding author

Vasilis Ntziachristos M.Sc. Ph.D.

Professor, School of Medicine and School of Electrical Engineering,

Director, Chair for Biological Imaging, (CBI); Technical University of Munich, Munich, Germany

Director, Institute for Biological and Medical Imaging (IBMI); Helmholtz Zentrum München, Neuherberg, Germany

Ingolstädter Landstr. 1, 85764 Neuherberg,

E-mal: v.ntziachristos@tum.de

V. Ntziachristos has received funding by the Leibniz Prize 2013 (NT 3/10-1).

EGE de Vries, PJ van Diest and WPThM Mali has received funding by the Center for Translational Molecular Medicine, project MAMMOTH (grant 03O-201),

EGE de Vries has received funding by ERC Advanced grant OnQView and SG Elias by the Dutch Cancer Society KWF by a research fellowship.

Abstract

In vivo tumor labeling with fluorescent agents may assist endoscopic and surgical guidance for cancer therapy as well as create opportunities to directly observe cancer biology in patients. However, malignant and non-malignant tissues are usually distinguished on fluorescence images by applying empirically determined fluorescence intensity thresholds. Here we report the development of fSTREAM, a set of analytic methods designed to streamline the analysis of surgically excised breast tissues by collecting and statistically processing hybrid multi-scale fluorescence, color, and histology readouts toward precision fluorescence imaging. fSTREAM addresses core questions of how to relate fluorescence intensity to tumor tissue and how to quantitatively assign a normalized threshold that sufficiently differentiates tumor tissue from healthy tissue. Using fSTREAM we assessed human breast tumors stained in vivo with fluorescent bevacizumab at microdose levels Showing that detection of such levels is achievable, we validated fSTREAM for high-resolution mapping of the spatial pattern of labeled antibody and its relation to the underlying cancer pathophysiology and tumor border on a per patient basis. We demonstrated a 98% sensitivity and 79% specificity when using labelled bevacizumab to outline the tumor mass. Overall, our results illustrate a quantitative approach to relate fluorescence signals to malignant tissues and improve the theranostic application of fluorescence molecular imaging.

Introduction

Clinical translation of fluorescence agents that target cancer has the potential to guide surgical and endoscopy procedures, improving upon the limitations of human vision [1, 2]. Several studies have received regulatory approvals to administer non-FDA approved targeted fluorescent agents to humans (see ClinicalTrials.gov NCT01508572, NCT02113202, NCT01972373, NCT02129933, NCT01987375, NCT02415881). Applied topically or systemically, targeted fluorescence agents are expected to change the landscape of interventional guidance by steering biopsy, improving disease detection and driving accurate theranostics [3]. Several studies have recently demonstrated the potential of using targeted fluorescent reporters to guide human surgery and endoscopy [4] [5] [3] [6] [7].

In addition to intraoperative guidance, *in-vivo cancer staining* in patients scheduled for surgery or endoscopy may offer new insights in tumor physiology and agent bio-distribution. Contrary to tissue histopathology that uses *ex-vivo* staining, histological analysis of human specimen stained *in-vivo* can reveal functional characteristics of the tumor and its microenvironment associated with agent delivery, biodistribution and targeting, on a per-patient basis and at resolutions not availabe to macroscopic optical imaging or radiological imaging.

However, an important and so far unsolved problem in in-*vivo* fluorescence cancer imaging is the uncertain relation of fluorescence intensity to the underlying tumor extent. Fluorescence images obtained *in-vivo* are diffusive (low resolution) in nature and do not delineate tumors with precision. Consequently, it becomes challenging to set an unbiased fluorescent threshold which will allow explicit differentiation of malignant from healthy tissue. As fluorescence molecular imaging is increasingly considered for clinical application, it becomes critical to develop methods

that lead to accurate tissue classification and reveal the relation between administered agent and tumor extent.

In this work we developed an analytical method that sought to deliver, objective criteria for fluorescence-based disease detection and differentiation from non-diseased tissues, toward precision fluorescence imaging. The study was based on clinical molecular imaging of breast cancer using fluorescence-labeled bevacizumab and had three objectives. First, it sought to establish the spatial relationship between the distribution of the antibody and the underlying tumor spatial extent, as it relates to the intraoperative identification of human breast cancer and cancer margins and quantitatively identify a fluorescence threshold for distinguishing malignant from non-malignant tissue. Of particular interest herein was the development of a fluorescence threshold that is normalized, i.e. it is not affected by variations of the amount of agent administered or agent dilution variations in each patient. Second, it inquired, in high-resolution, the spatial-pattern of labeled antibody within human cancer, a parameter not previously resolved by radiological methods and generally unknown due to the effects of interstitial pressure gradients and abnormal tumor vascularization. Finally, the study identified the sensitivity and specificity of cancer detection using bevacizumabIRDye800CW and quantified the ability to detect fluorescent agents administered at micro-dosing amounts. The underlying threshold analysis and biodistribution study was part of a clinical molecular imaging study of breast cancer using fluorescence-labeled bevacizumab in 20 patients with breast cancer of whom 19 patients were eligible for analysis. Tracer application was concluded to be safe and details are described in Lamberts et al [1]

Methods

Clinical study

We administered bevacizumab conjugated to the near-infrared (NIR) fluorescent dye IRDy800CW (i.e. bevacizumab-IRDye800CW) to breast cancer patients. Drug labelling was achieved at the University Medical Center Groningen under therein established Good Manufacturing Practices (GMP) [2] . Bevacizumab-IRDye800CW is already considered in clinical trials for surgical and endoscopic guidance (ClinicalTrials.gov numbers: NCT01508572, NCT01972373 and NCT02113202). Nineteen patients diagnosed with breast cancer at mean age 64.6 years (10.26 years standard deviation) have been included in this analysis. Tumor sizes, evaluated at pathology, averaged at 20.1mm (7.9mm standard deviation). Consistent with micro-dosing regulations, as described in the FDA guidelines "Guidance for Industry, Investigators, and Reviewers Exploratory IND Studies", 4.5mg of labeled bevacizumab (<30nMol of labelled antibody) were administered to patients three days prior to surgery (see supplementary section for details).

Development of fSTREAM

To achieve the study objectives, we developed comprehensive analysis of fluorescent human tissue specimen at multiple scales (Fig.1). Termed *f*STREAM, the analysis co-registers 1) color images, 2) fluorescence images, 3) H&E mosaic stained microscopy slices and 4) the pathologists demarcation border obtained from an excised cancer specimen, onto a common geometrical frame. Subsequently, statistical processing of the 4-modal hybrid image was carried-out to guide threshold selection by studying bevacizumab-IRDye800CW distribution in human breast cancer. The study obtained multi-scale measurements from tissue specimen at the macroscopic, mesoscopic and microscopic scales, i.e.

Macroscopic tumor imaging, based on a real-time color and fluorescence composite EagleRay-V3 camera, custom-developed at the Helmholtz Zentrum München (HMGU) and Technical University of Munich (TUM) [3], [4] (see Suppl. Material) and approved for clinical use by the IRB Board of the University Medical Center Groningen. EagleRay-V3 video and images

were simultaneously acquired during surgery (Fig.1b) at a field of view (FOV) of ~15 cm x 15 cm and resolution of 150 microns. Immediately after the excision, the surgical specimen was placed on a table and imaged (Fig.1c) with the same EagleRay-V3 parameters.

Mesoscopic EagleRay-V3 color and fluorescence imaging was then performed on freshly excised 3mm-thick lamellae (Fig.1e) using mesoscopic parameters, i.e. 2cm x 2cm FOV and 20 micrometer resolution. Shortly after, the lamellae were fixed in paraffin. Paraffin blocks were also imaged with mesoscopic imaging settings (Fig.1f) using the EagleRay-V3 camera or flat-bed scanning (Odessy, Licor Nebraska). Details are outlined in the Supp. Material "Fluorescence validation, H&E & VEGF-A Staining".

Microscopic mosaicking imaging was then performed on consecutive 4-micron thick histological slices obtained from the paraffin blocks, covering the same field of view as in mesoscopic imaging (Fig.1g). The histology slices were stained with H&E and tumor demarcation was performed by experienced pathologists. All pathologists were blinded to the fluorescence signals during the classification process. Interleaved histology slices not processed by H&E were stained for VEGF-A expression using the polyclonal IgG VEGF A-20 Antibody (sc-152, Santa Cruz Biotechnology, Santa Cruz, USA) and imaged with conventional microscopy. (For details see Suppl. Material section "Fluorescence validation, H&E & VEGF-A Staining").

Color and fluorescence images, obtained from paraffin blocks, were registered onto the corresponding H&E mosaic image obtained from the same field of view. Then the pathologists' tumor segmentation on the H&E image was recorded and registered on the color, fluorescence and H&E images. Image registration was based on affine transformations utilizing six or more anatomical landmarks. The 4-modality coregistration was an essential *f*STREAM step in order to *streamline* the spatial and intensity correlations between malignant tissue area and fluorescence signals.

Identification of a global threshold

The work herein sought to develop a method that could derive an objective, quantitative global threshold for optimal cancer delineation. The use of a normalized objective global threshold is critical for the clinical application of fluorescence imaging, i.e. at conditions where real-time guidance is required. The following analysis was applied to the bevacizumab-IRDye800CW breast cancer study treated herein. Nevertheless, the proposed methodology is generalizable to any fluorescence imaging study.

The first step in deriving a normalized global threshold was image normalization, so that threshold application relates to comparable images independently of gains (intensity of illumination, camera amplification), background noise (ambient light, read noise etc) and tissue variations or amount of agent administered and patient body weight. We therefore assumed the normalized fluorescence image S_i, i.e.,

$$S_{ij}(\alpha,\beta,\gamma) = \frac{F_{ij}}{\alpha * mean(F_i) + \beta * thres(F_i)} + \gamma \quad , \qquad \text{Eq.1}$$

whereby $F_{i,j}$ is the fluorescence intensity value of the j-th pixel of the i -th image of the original (raw) fluorescence image, assuming a number of fluorescence images i =1..N obtained from different patients (e.g. Fig. 2e or 3b). The parameters α, β modulate the normalization of image *Fi* by its mean value *mean(F_i)* and a threshold value *thres(F_i)*; the latter indicating the value that maximizes the inter-class variance for the i -th image and was determined by the Otsu's method [5] for each *Fi* image. The parameter γ adjusts the image offset, representative of a background constant value due to bias values typically present in CCD camera images. To derive a global threshold, we determined the values $[\alpha\ \beta\ \gamma]$ by minimizing the cost function C($[\alpha, \beta, \gamma]$) of, i.e. :

$$C(\alpha, \beta, \gamma) = (1 - AUC(S([\alpha, \beta, \gamma]), G)) \quad \text{Eq.2}$$

where G is a binary image indicating the areas of malignant vs. non-malignant tissue on the image S, as obtained by the congruent H&E pathology segmentation, and AUC is the area under the ROC curve (the normalized Mann-Whitney-Wilcoxon test). The optimal $[\alpha\ \beta\ \gamma]$ parameters used in image normalization (Eq.1) were estimated by an unconstrained nonlinear optimization.

ROC analysis

ROC analysis was performed on data from all specimen measured and processed by Eq.1, using the image normalization parameter set $[\alpha\ \beta\ \gamma]$ obtained by Eq.2. To inspect whether the use of a global threshold did not produce any outliers in the data set examined, we solved (minimized) Eq.2 21 times. Each time, the minimization utilized 21 samples to derive the global threshold and excluded a different sample from the training set.

Homogeneity of bevacizumab-IRDye800CW distribution

The study further examined the patterns of bevacizumab-IRDye800CW in human breast cancer. To quantify the spatial pattern observed, we calculated entropy values for areas of $(0.5\text{mm})^2$ on the raw fluorescence tumor images obtained from the paraffin blocks. The bevacizumab-IRDye800CW distribution pattern at a higher resolution was also interrogated by analyzing images acquired from 4 μm slices obtained from each of the 3mm-thick lamellas employed for the entropy analysis.

Results

Pattern of bevacizumab-IRDye800CW distribution in breast cancer

Fluorescence images obtained *in situ* or post-surgery from excised specimen (Fig.2a,b) exhibited patterns of diffusive appearance. In breast cancer surgery a positive margin is defined as 'ink-on-tumor' according to the 2014 SSO/ASTRO guidelines [6], however, a margin of several millimeters to centimeters is allowed around the tumor to ensure complete tumor resection. Therefore, diffusive appearance of fluorescence signals indicated a complete (R0) resection, i.e. no ink on tumor. Signals from tumors as deep as at least 1cm could be nevertheless detected (Fig.2b).

Mesoscopic imaging of lamelae (Fig.2c) offered first insights into the distribution parameters of the fluorescent bevacizumab. We observed an apparent, previously undisclosed *homogenous* distribution of bevacizumab-IRDye800CW throughout the tumor area. The images were obtained according to the step in Fig.1f and demonstrate that sufficient fluorescence signal could be collected even after paraffin preservation. Occasionally, the processing of human tissue into lamellae would tear tissue in areas of low structural integrity, typically associated with necrotic areas in the tumor center, giving an appearance of openings in the middle of the tumor. Fig. 2d,e show images from a paraffin embedded specimen from the rectangular area marked on Fig. 2c. These findings suggest that bevacizumab-IRDye800CW distributed in a diffusive manner throughout the tumor mass, apparently without strong influence by tumor interstitial fluid pressure or irregular perfusion (See also Fig.3 and Fig.4). The fluorescence images of the lamellae contain light scattering effects due to the sample thickness of 3 mm; therefore the images in Fig.2 are diffusive in nature. This is evidenced by inspecting fluorescence intensity profiles. Even though the borderline between tumor and healthy tissue on histological slices is marked by pathologists as a sharp line (Fig.2f), the fluorescence signals, as expected, do not exhibit sharp borders but a diffuse appearance with no distinct definition of the tumor margin(Fig.2i, j).

Relation of bevacizumab-IRDye800CW distribution and breast cancer

A next step was to quantitatively relate bevacizumab-IRDye800CW distribution to malignant tissue. Results from patient #8 are shown on Fig. 3a-e for demonstration purposes. Color and fluorescence images (Fig.3a, b) from the paraffin blocks were registered onto the corresponding H&E mosaic image (Fig.3d) and the pathologists' tumor segmentation (Fig.3e), based on affine transformations (see methods). Raw fluorescence counts from the tumor and background tissue for patient #8 are shown on Fig.3f, indicating a target (tumor) to background ratio of ~2.5.

The tumor to background ratio for the entire sample analyzed was related to the pathological Bloom–Richardson–Elston (BRE) tumor grade (Fig. 3g). The BRE is a breast cancer classification metric that indicates cancer aggressiveness and combines measurements of the severity of tubule formation, nuclear pleomorphism and mitotic count per area in the tumor sample analyzed. We observed that tumors of pathological grade score 1 exhibited less fluorescence uptake compared to tumors of grade 2 and 3. Overall, the TBR values ranged from 1.8 to 9. Fluorescence signals from the paraffin sections of all patients were spatially correlated to the underlying cancer area identified on the co-registered H&E slices. A Receiver-Operator-Characteristic curve was drawn for each patient sample, assuming different thresholds (Fig.3h).

Histological confirmation was corroborated by immunohistochemistry staining for VEGF-A expression, performed on interleaved paraffin sections of 4μm thickness (Fig.3i-f). Elevated VEGF-A expression (Fig.3k) was shown for the tumor area but not for surrounding non-malignant tissue (Fig.3l).

Application of a Global threshold

Fig.3h depicted the ROC curve for each patient and presented the sensitivity and specificity by which fluorescence intensity patterns demarcate the tumor area, as confirmed by

H&E analysis. However a critical parameter in interventional fluorescence imaging relates to setting an intensity threshold on the fluorescence image in order to differentiate cancer from healthy tissue, in the absence of an H&E analysis. Today, thresholds are empirically assigned based on image appearance and may inaccurately estimate the tumor extent and surrounding tissue (see Fig.4a-d).

The derivation of an objective normalized global threshold (see methods) determined the optimal $[\alpha\ \beta\ \gamma]$ parameters (see Eq.1, 2), which were estimated to be [0.9240, 1.3103, 0.0040] for the set of 22 paraffin block samples from the 19 patients examined (double paraffin samples were available in pathology from 3 patients with large tumors). The ROC analysis considered all specimen images processed by Eq.1 using image normalization based on the optimal parameter set $[\alpha\ \beta\ \gamma]$. The resulting ROC curve (Fig.4e) achieved an Area Under the Curve (AUC) value of 0.97 for all 22 samples examined. We note that skin regions exhibited elevated fluorescence but were not included in the analysis (see Fig.1 in Suppl. Material for details). To confirm the generality of the global threshold, we computed the AUC variation between an excluded sample and the remaining set of samples (see methods). The AUC variation was ± 0.00389%, indicating that the application of the global threshold did not produce any outliers in any of the data sets examined.

Homogeneity of bevacizumab-IRDye800CW distribution

Fig. 2 and 3 showcased a rather homogeneous distribution of bevacizumab-IRDye800CW throughout tumors. Entropy calculations (see methods) quantified the spatial pattern observed on the raw fluorescence tumor images from paraffin blocks (Fig. 4f). The mean entropy value for all patient samples was 3.06 with a standard deviation of ± 0.81 for a $(0.5\text{mm})^2$ neighborhood; a finding that confirms a homogeneous pattern of labeled drug distribution in all patient samples examined

Entropy analysis of 4 μm slices obtained from each of the 3mm-thick lamellas employed was also considered for higher-resolution bevacizumab-IRDye800CW observations, since images from the 4 μm slices are virtually scatter-free. The corresponding voxels represented on Fig.4g are of lower total volume compared to the voxels observed in Fig. 4a-c. The entropy value for a $(0.5mm)^2$ area within tumors was 6.4374 ± 0.81006. As expected, the entropy increases when observing higher resolution images, but nevertheless showcases also a homogeneous distribution, which remains overtly constant from patient to patient. We further observed that even in high-resolution view, the fluorescence pattern generally matched the H&E outlined tumor border, although it marginally overestimated the tumor border (fig.4d). A comparison of magnified views from 4μm-thick vs. paraffin block images is shown in (Suppl. Fig. 2).

Discussion

fSTREAM was proposed as methodology for standardized analysis of fluorescence images obtained from tissues after the administration of fluorescent agents *in-vivo*. The method was applied to analyze breast cancer specimen labelled with Bevacizumab-IRDye800CW, obtained from a Phase I clinical trial and guide the selection of a normalized objective global threshold, i.e. a single normalized value derived to optimally separate malignant tissue from surrounding healthy tissue in the entire study. It was found that derivation of an objective global threshold required appropriate image normalization, performed by Eq.1, so that the intensity seen on different images is calibrated to the same reference (standard). The derivation of a normalized threshold further ensures a metric that is independent of the exact amount of agent administered, patient body weight or absolute fluorescence intensity values, since it classifies tissues based on relative intensities and in relation to the overall image statistics (Eq.1). It is nevertheless expected that the *fSTREAM* analysis is applied on a per-study basis, since the threshold value will depend on the particular type of tracer employed and possibly the tissue type targeted. Therefore, data collected

during a Phase I study conducted for a new tracer could be analyzed to derive a threshold for use in subsequent exploratory phases or during interventional procedures. Naturally, additional data obtained from Phase II/III studies may be retrospectively used to further optimize the threshold.

The proposed methodology does not involve modification of the specimen analyzed, since it utilizes samples in paraffin blocks and conventional histology slices, therefore it can be seamlessly incorporated into the routine histopathological analysis workflow.

Today, fluorescence images using targeted agents are evaluated based on the assumption that stronger signal implies malignancy. Correspondingly, it is typical to render the stronger fluorescence intensities of a fluorescence image in pseudocolor, together with a color image as shown in Fig.3c. This rendering operation implies the application of a threshold on the fluorescence image depicted. However, due to the diffusive nature of fluorescence photons collected from tissues, the exact relation of fluorescence intensity / threshold and malignancy is not known; thresholds are typically user-dependent, empirical in nature and therefore prone to errors. Observations of Fig.2g-j showcase that there exists no clear border for cancer differentiation when performing fluorescence imaging of tissues, due to photon diffusion effects that reduce the resolution of the fluorescence image. Therefore the selection of an objective global threshold is critical for the clinical application of fluorescence imaging, especially in association of guiding cancer resection and observing for tumor borders.

A central *fSTREAM* target was the rigorous relation of fluorescence signals to cancer. Therefore, an important parameter in the analysis proposed was the co-registration of the tumor demarcation by pathologists on H&E slices and corresponding fluorescence images. Affine transforms allowed a per-pixel analysis of fluorescence intensities and the underlying presence of malignant vs. non-malignant cells. Then automatic statistical analysis on a pixel-to-pixel basis

enabled accurate and statistically significant correlation between pathological classification and tumor-to-background- fluorescence intensity ratios.

The analysis intrinsically also observed the unknown distribution pattern of Bevacizumab-IRDye800CW in human breast cancer, demonstrating broad presence in the entire tumor mass. We confirmed that the labeled drug can be detected at micro-dosing amounts (30nMol per patient) and can be assessed at macroscopic and mesoscopic scales. ROC analysis calculated a sensitivity of 98% and a specificity of 79% when using fluorescence signals to outline the tumor mass. Breast cancer surgery is reported to yield up to ~30% positive tumor margins, directing secondary procedures [7]. Hence, the findings herein preliminary showcased that Bevacizumab-IRDye800CW may be valuable for intraoperative breast cancer margin detection, a hypothesis which is currently investigated in a follow-up phase II clinical study (ClinicalTrials.gov Identifier: NCT02583568). It was suggested that fluorescent bevacizumab selectively labels cancer in xenograft animals [8] and can be employed for imaging studies, even if it only targets soluble VEGF-A [9] [10]. Staining for VEGF-A expression revealed elevated VEGF levels in all tumors studied herein. Nevertheless, it is likely that the homogeneous distribution pattern observed is influenced by enhanced permeability and retention effects.

We also observed Bevacizumab-IRDye800CW presence in areas not rich in VEGF expression including the skin and breast ducts. The sensitivity and specificity data reported were calculated only for the area (volume) around the tumor, as defined by the surgical specimen, not for the entire breast tissue, and it therefore relates more closely to intra-operative observations and not breast cancer diagnosis in the radiological sense.

Labeled drugs have been considered for imaging studies due to their general availability and expectation that the bio-distribution and targeting profile of the labelled molecule will not

significantly vary over the unlabeled counterpart, especially when labeling antibodies [11]. [12] [13]. Radionuclide-labeled drugs are often assessed with Positron Emission Tomography to quantitatively determine the dose of an administered therapeutic molecule delivered into different organs, whereas other, non-therapeutic molecules are considered for diagnostic and staging purposes [14] [15]. Examples include imaging of anti-folate agents [16] or monoclonal antibodies [8] [10]. However, while nuclear imaging studies enable full-body scans, the low spatial resolution achieved only allows assessment of the macro-distribution at volume sampling of ~0.1 - 1 cm3 [17]. *fSTREAM* comes with the potential to study the labeled molecule at higher-resolution, within the tumor micro-environment and better understand long-term bio-distribution within the cancer lesion, albeit it can only be applied as an invasive technique within surgery and endoscopy

Overall, fSTREAM can be employed for the systematic analysis of new classes of fluorescent agents considered for human use and broader disease targets [8] [11]. Moreover, it can be considered as an alternative method to elucidate human cancer biology by observing personalized readings of cancer pathophysiology on excised specimen following fluorescence-guided procedures using targeted agents. The high sensitivity of the method allows micro-dosing observations, possibly relaxing regulatory parameters. Such application could capitalize on the emerging clinical practice of using fluorescent agents for diagnostic purposes[18] [19] [20] [21] [22].

REFERENCES

1. Lamberts LE, Koch M, de Jong JS, Adams A, Glatz J, Tranendonk MEG, Terwisscha van Scheltinga AGT, Jansen L, de Vries J, Lub-de Hooge MN, et al: **Tumor-specific uptake of fluorescent bevacizumab-IRDye800CW microdosing in patients with primary breast cancer: a phase I feasibility study.** *Clinical Cancer Research* 2016.
2. ter Weele EJ, van Scheltinga AGT, Linssen MD, Nagengast WB, Lindner I, Jorritsma-Smit A, de Vries EG, Kosterink JG, Lub-de Hooge MN: **Development, preclinical safety, formulation, and stability of clinical grade bevacizumab-800CW, a new near infrared fluorescent imaging agent for first in human use.** *European Journal of Pharmaceutics and Biopharmaceutics* 2016, **104:**226-234.
3. Themelis G, Yoo JS, Soh K-S, Schulz R, Ntziachristos V: **Real-time intraoperative fluorescence imaging system using light-absorption correction.** *Journal of biomedical optics* 2009, **14:**064012-064012-064019.
4. Glatz J, Varga J, Garcia-Allende PB, Koch M, Greten FR, Ntziachristos V: **Concurrent video-rate color and near-infrared fluorescence laparoscopy.** *Journal of biomedical optics* 2013, **18:**101302-101302.
5. Otsu N: **A threshold selection method from gray-level histograms.** *Automatica* 1975, **11:**23-27.
6. Moran MS, Schnitt SJ, Giuliano AE, Harris JR, Khan SA, Horton J, Klimberg S, Chavez-MacGregor M, Freedman G, Houssami N: **SSO-ASTRO consensus guideline on margins for breast-conserving surgery with whole breast irradiation in stage I and II invasive breast cancer.** *International journal of radiation oncology, biology, physics* 2014, **88:**553.
7. Houssami N, Macaskill P, Marinovich ML, Morrow M: **The association of surgical margins and local recurrence in women with early-stage invasive breast cancer treated with breast-conserving therapy: a meta-analysis.** *Annals of surgical oncology* 2014, **21:**717-730.
8. Nagengast WB, de Vries EG, Hospers GA, Mulder NH, de Jong JR, Hollema H, Brouwers AH, van Dongen GA, Perk LR, Lub-de Hooge MN: **In vivo VEGF imaging with radiolabeled bevacizumab in a human ovarian tumor xenograft.** *Journal of Nuclear Medicine* 2007, **48:**1313-1319.
9. Nayak TK, Garmestani K, Baidoo KE, Milenic DE, Brechbiel MW: **PET imaging of tumor angiogenesis in mice with VEGF-A–targeted 86Y-CHX-A ″-DTPA-bevacizumab.** *International Journal of Cancer* 2011, **128:**920-926.
10. Nagengast WB, Lub-de Hooge MN, Oosting SF, den Dunnen WF, Warnders F-J, Brouwers AH, de Jong JR, Price PM, Hollema H, Hospers GA: **VEGF-PET imaging is a noninvasive biomarker showing differential changes in the tumor during sunitinib treatment.** *Cancer research* 2011, **71:**143-153.
11. Scheuer W, van Dam GM, Dobosz M, Schwaiger M, Ntziachristos V: **Drug-based optical agents: infiltrating clinics at lower risk.** vol. 4. pp. 134ps111-134ps111: American Association for the Advancement of Science:134ps111-134ps111.
12. van Oosten M, Schäfer T, Gazendam JA, Ohlsen K, Tsompanidou E, de Goffau MC, Harmsen HJ, Crane LM, Lim E, Francis KP: **Real-time in vivo imaging of invasive- and biomaterial-associated bacterial infections using fluorescently labelled vancomycin.** *Nature communications* 2013, **4**.

13. Rosenthal EL, Warram JM, de Boer E, Chung TK, Korb ML, Brandwein-Gensler M, Strong TV, Schmalbach C, Morlandt A, Agarwal G: **Safety and Tumor-specificity of Cetuximab-IRDye800 for Surgical Navigation in Head and Neck Cancer.** *Clinical Cancer Research* 2015**:**clincanres. 3284.2014.
14. Van de Wiele C, Lahorte C, Oyen W, Boerman O, Goethals I, Slegers G, Dierckx RA: **Nuclear medicine imaging to predict response to radiotherapy: a review.** *International Journal of Radiation Oncology* Biology* Physics* 2003, **55:**5-15.
15. Heusner T-A, Kuemmel S, Koeninger A, Hamami ME, Hahn S, Quinsten A, Bockisch A, Forsting M, Lauenstein T, Antoch G: **Diagnostic value of diffusion-weighted magnetic resonance imaging (DWI) compared to FDG PET/CT for whole-body breast cancer staging.** *European journal of nuclear medicine and molecular imaging* 2010, **37:**1077-1086.
16. Kamen BA, Smith AK: **A review of folate receptor alpha cycling and 5-methyltetrahydrofolate accumulation with an emphasis on cell models in vitro.** *Advanced drug delivery reviews* 2004, **56:**1085-1097.
17. Moses WW: **Fundamental limits of spatial resolution in PET.** *Nuclear Instruments and Methods in Physics Research Section A: Accelerators, Spectrometers, Detectors and Associated Equipment* 2011, **648:**S236-S240.
18. Stanga PE, Lim JI, Hamilton P: **Indocyanine green angiography in chorioretinal diseases: indications and interpretation: an evidence-based update.** *Ophthalmology* 2003, **110:**15-21.
19. Schaafsma BE, Mieog JSD, Hutteman M, Van der Vorst JR, Kuppen PJ, Löwik CW, Frangioni JV, Van de Velde CJ, Vahrmeijer AL: **The clinical use of indocyanine green as a near-infrared fluorescent contrast agent for image-guided oncologic surgery.** *Journal of surgical oncology* 2011, **104:**323-332.
20. Jallad KN, Kennedy MD, Low PS, Ben-Amotz D: **Folate targeted enhanced tumor and folate receptor positive tissue optical imaging technology.** Google Patents; 2014.
21. Weber CJ, Müller S, Safley SA, Gordon KB, Amancha P, Villinger F, Camp VM, Lipowska M, Sharma J, Müller C: **Expression of functional folate receptors by human parathyroid cells.** *Surgery* 2013, **154:**1385-1393.
22. Sun JY, Shen J, Thibodeaux J, Huang G, Wang Y, Gao J, Low PS, Dimitrov DS, Sumer BD: **In vivo optical imaging of folate receptor-β in head and neck squamous cell carcinoma.** *The Laryngoscope* 2014, **124:**E312-E319.

Tables

Sensitivity:	Specificity	Threshold of S (presentence of maximum normalized fluorescence value)
0.9000	0.9274	13.2%
0.9500	0.8775	9.8%
0.9800	0.7882	6.5%

TABLE 1: Global sensitivity and specificity values.

Figure Legends:

Figure 1:

*f*STREAM imaging pipeline from in-situ/in-vivo macroscopy to *ex vivo* mesoscopy and microscopy. (a) Bevacizumab-IRDye800CW was systemically administered to breast cancer patients 72 hours before surgery. (b) Macroscopic real-time fluorescence and color epi-illumination images were acquired during surgery and (c) from excised breast tissue ~5min post-surgery: (field of view of 10cm x 10cm). (d) Excised tissue was subsequently cut to 3mm lamellae and casted in 2 cm x 3cm blocks embedded into paraffin. (e) Mesoscopic imaging of fresh excised lamellae was performed immediately after step (d). (f) Paraffin embedded tissue blocks were then imaged with a 2cm x 2cm field of view and 20 micrometer resolution. (g) Mosaicking H&E microscopic imaging was then performed on 4-micron slices obtained from the paraffin blocks imaged in step (f). Histological imaging was also performed on slices stained for VEGF.

Figure 2:

Spatial patterns of bevacizumab-IRDye800CW distribution in an invasive ductal carcinoma (a) Color and **(b)** hybrid color and fluorescence image of deep-seated breast tumor during a mastectomy in situ. The fluorescence signal is overlaid in cyan pseudo-color onto the color reflectance image. **(c)** Fresh lamella of 3mm thickness obtained from breast tissue specimen containing a tumor. The tumor is marked in this view with a green pseudo-color. Note that this image is taken directly from a cut through the tumor and the signal exhibits much less diffusion than in Fig. 2b. Necrosis has developed in the core of the tumor. The scale bar is 10 mm. **(d)** Color image of the paraffin-embedded tissue sample obtained from an area delineated on (c) by a white rectangle. The scale bar is 5 mm. **(e)** Fluorescence image of the same area overlaid in green pseudo-color on the color image shown in (d). **(f)** H&E staining of 4μm-thick paraffin slice corresponding to the field of view in (d). The green dotted line marks the tumor border

according to histopathology. The scale bar in (d,e,f) is 5 mm. **(g)** Magnifications of color , **(h)**pseudo-color overlay and **(i)**raw fluorescence images obtained from the region outlined by the rectangle in subfigure (c) **(j)** Fluorescence intensity profile along the blue line shown in (i) High fluorescence photon diffusion is visible on the images leading to an uncertain tumor border delineation.

Figure 3:

Image co-registration, target-to-background analysis and spatial correlation of fluorescence and histological data. Images in panels (a) - (e) were registered to each-other by affine transformation based on (>6) morphological features. **(a)** Color image of the examined paraffin sample from a patient. **(b)** Fluorescence image of the same view. **(c)** Alpha-blending overlay of pseudo colored fluorescence signal and color reflectance image. **(d)** Corresponding H&E staining of the same speciment. **(e)** Tumor location according to pathology outline. Gray color indicates background tissue. Purple color indicates malignant areas. The scale bar in (a)- (e) is 5 mm (**f)** Box plot of signal distribution of background region (left box) vs. tumor region (right box) for the sample in Fig.3.a,-(e). (**g)** Scatter plot of tumor to background ratios versus pathological grading for all patient samples; the red lines show the mean for each pathological grading group. The 95% confidence interval is marked in pink while 1 standard deviation is colored in blue. (**h)** Receiver-operator-characteristics for all patient samples revealing the performance of a pure value-driven binary classification in means of sensitivity vs. specificity. (**i, j)** Magnified view of H&E stained tumor region and non-cancerogenous tissue, respectively. **(k)** Corresponding VEGF-A20 staining of tumor region and **(l)** corresponding VEGF-A20 staining of non-tumor tissue region. The VEGF-expression is stained in brown; hematoxylin performs cell counterstaining for reference. The scale bar in (i)-(l) is 50 μm.

Figure 4:

Influence of threshold on segmentation. **(a) – (c)** Fluorescence images of paraffin embedded tissue block obtained from breast cancer stained in vivo with Bevacizumab-IRDye800CW. The region of interest (ROI) selected for different threshold levels are marked by the red line. The

scale bar is 2mm **(d)** H&E stained slice with the gold standard segmentation by a pathologist in green and the calculated segmentation based on the fluorescence image in blue, for the threshold used in (c). **(e)** Receiver-Operator-Characteristics for all paraffin blocks when using the proposed global threshold achieving an AUC of 0.97. **(f)** Distribution of the entropy values on a $(0.5mm)^2$ neighborhood of all segmented tumor regions of paraffin block fluorescence images. The black dots represent single entropy values. The red line shows the mean value. The 95% confidence interval is marked in pink while 1 standard deviation is colored in blue. The data is jittered and subsampled for visualization. The low entropy values illustrate the high homogeneity in this paraffin block image. **(g)** Fluorescence image of 4μm-thick slice corresponding to (a) – (c) obtained from breast cancer stained in vivo with Bevacizumab-IRDye800CW. The scale bar is 2mm.

Figure 1

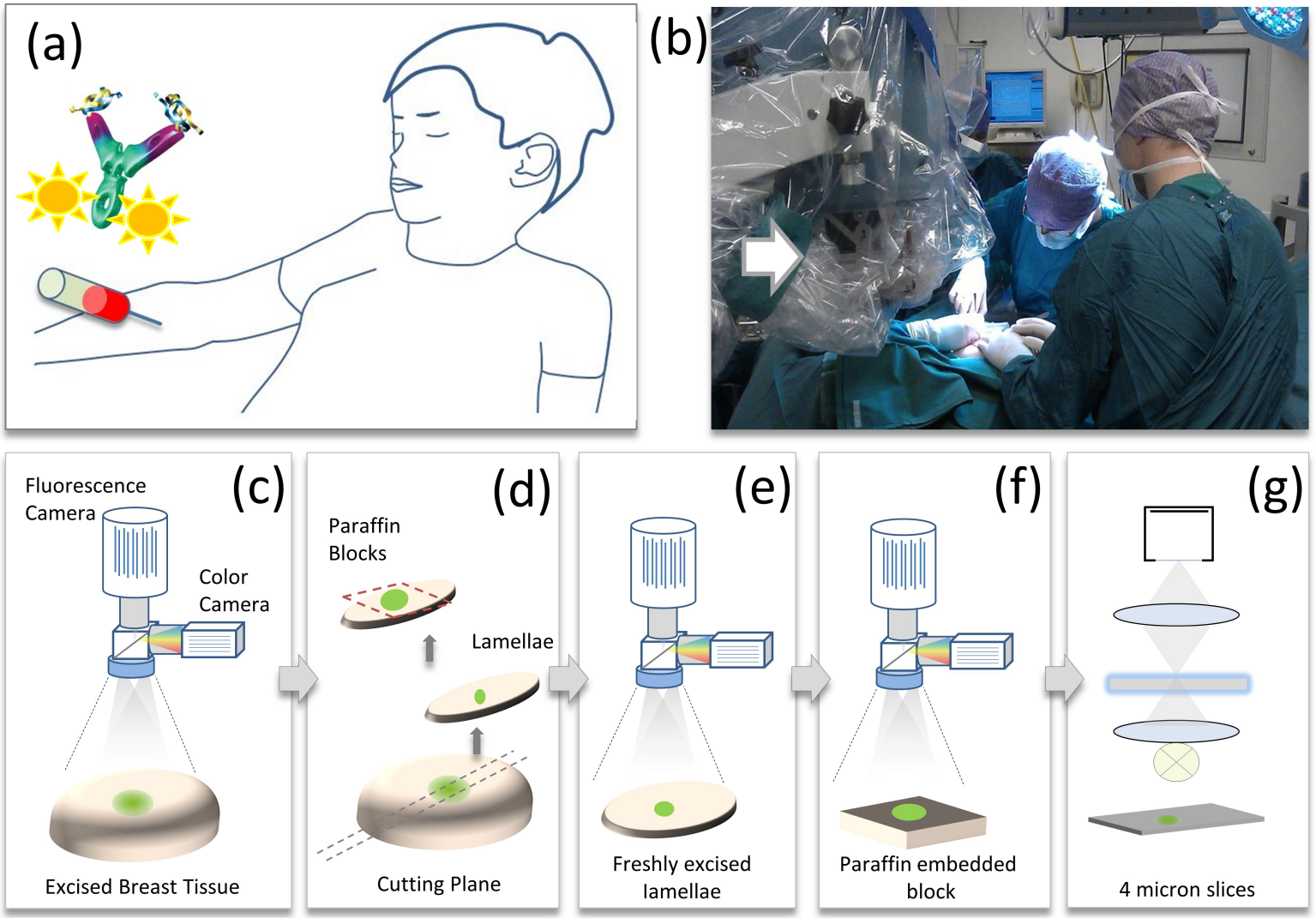

Time	5 min	1h	24h	28h
Resolution	150 µm	150 µm	20µm	0.5µm
FoV	15c15 cm²	15x15 cm²	2x2 cm²	1x1 cm²

Figure 2

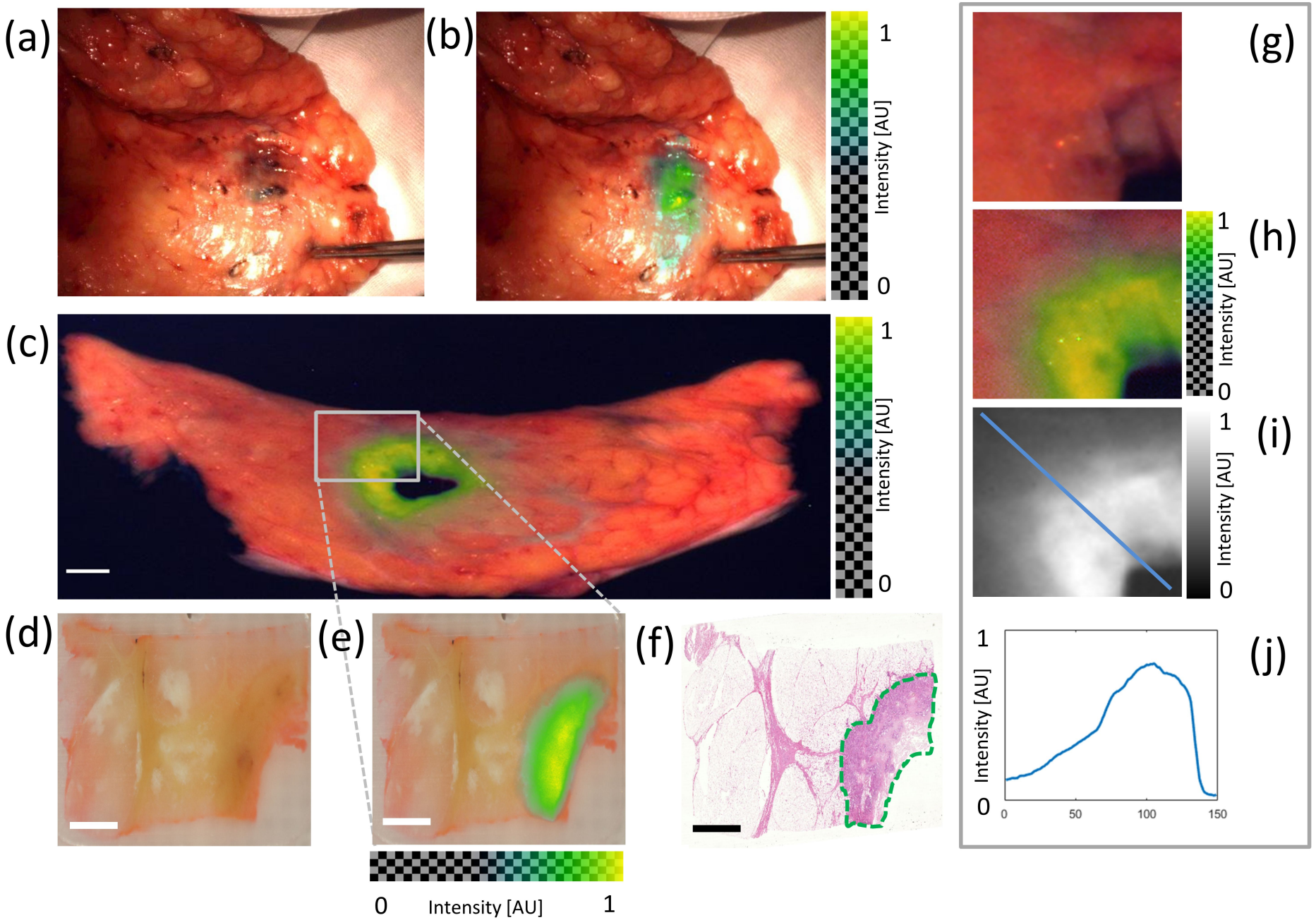
(a)
(b)
1
Intensity [AU]
0
(c)
1
Intensity [AU]
0
(d)
(e)
0
Intensity [AU]
1
(f)
(g)
(h)
1
Intensity [AU]
0
(i)
1
Intensity [AU]
0
(j)
1
Intensity [AU]
0
0
50
100
150

Figure 3

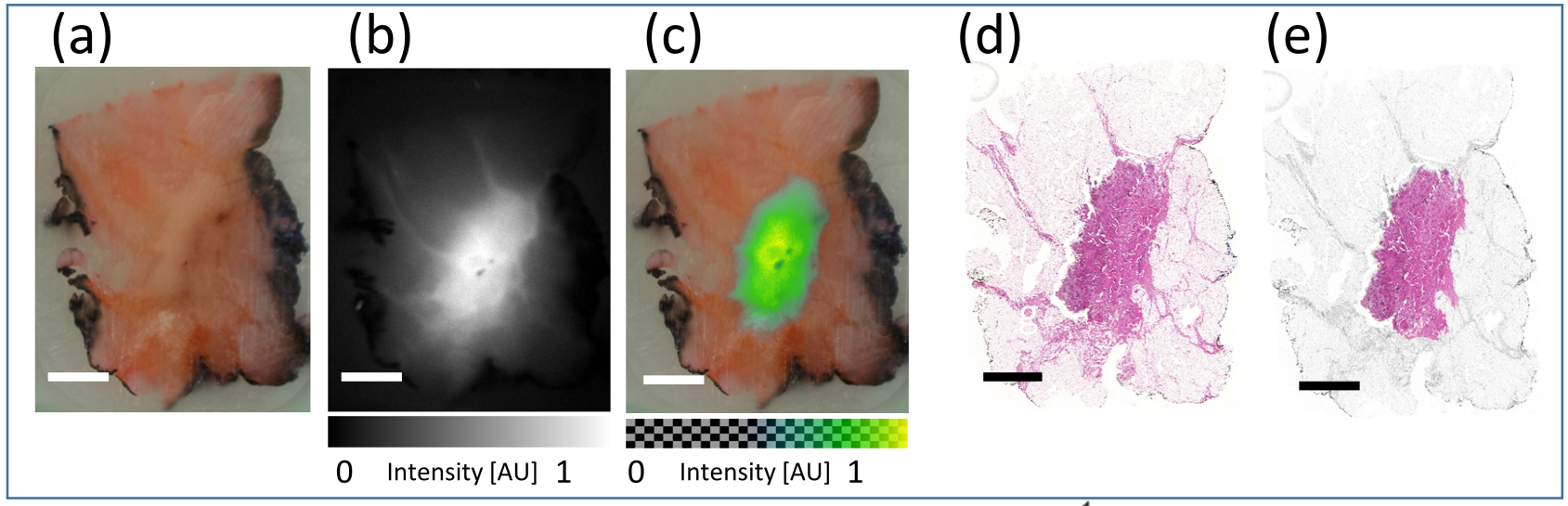
(a)
(b)
(c)
(d)
(e)
0 Intensity [AU] 1
0 Intensity [AU] 1

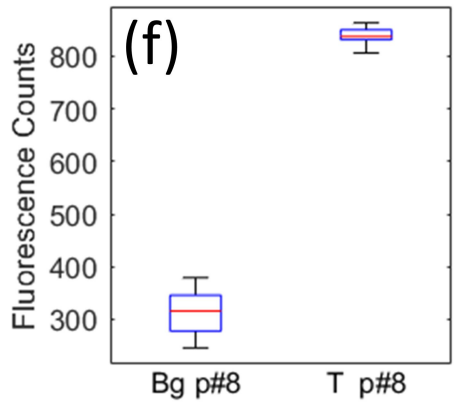
(f)
Fluorescence Counts
800
700
600
500
400
300
Bg p#8
T p#8

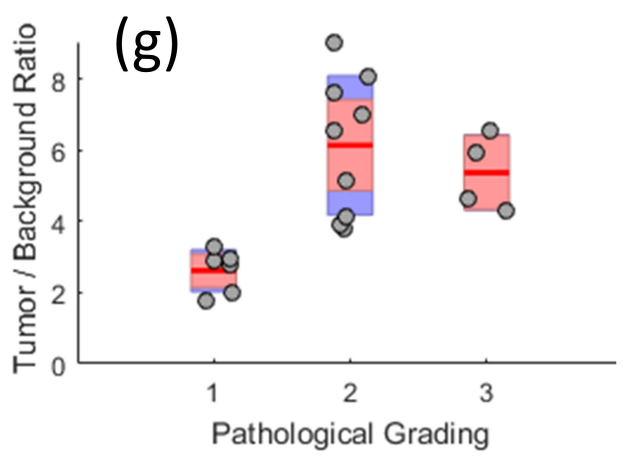
(g)
Tumor / Background Ratio
8
6
4
2
0
1
2
3
Pathological Grading

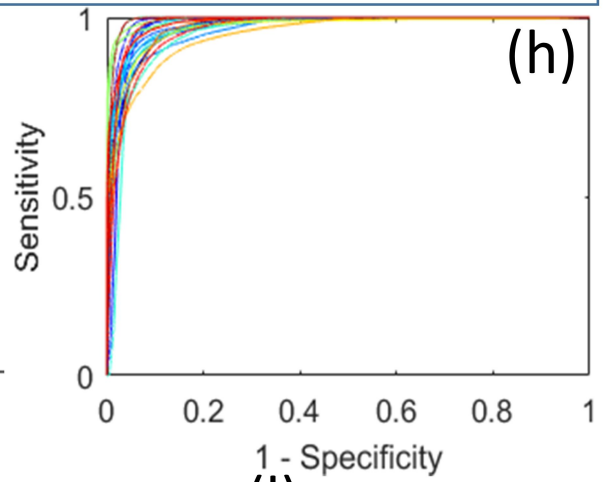
(h)
Sensitivity
1
0.5
0
0
0.2
0.4
0.6
0.8
1
1 - Specificity

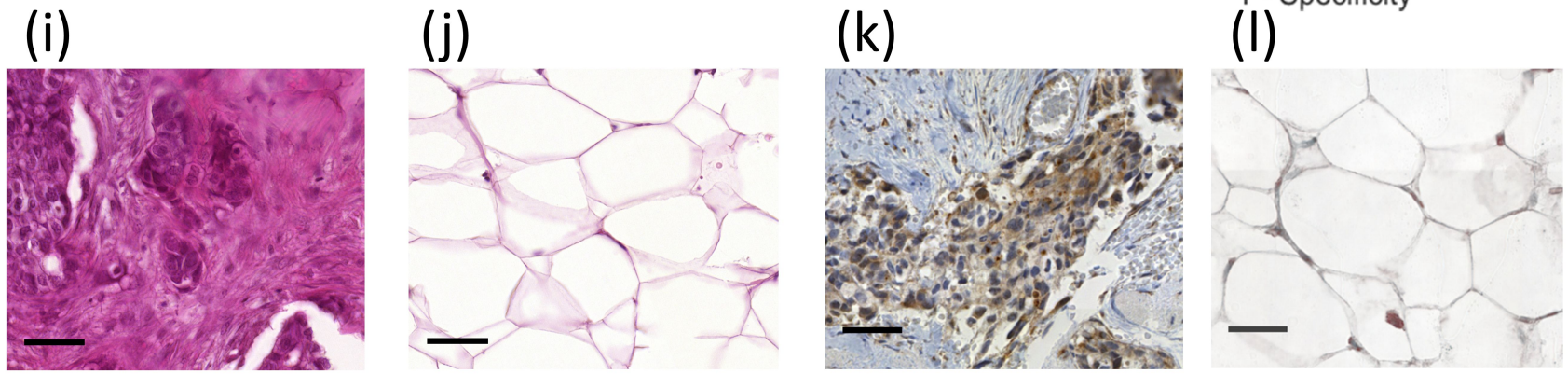
(i)
(j)
(k)
(l)

Figure 4

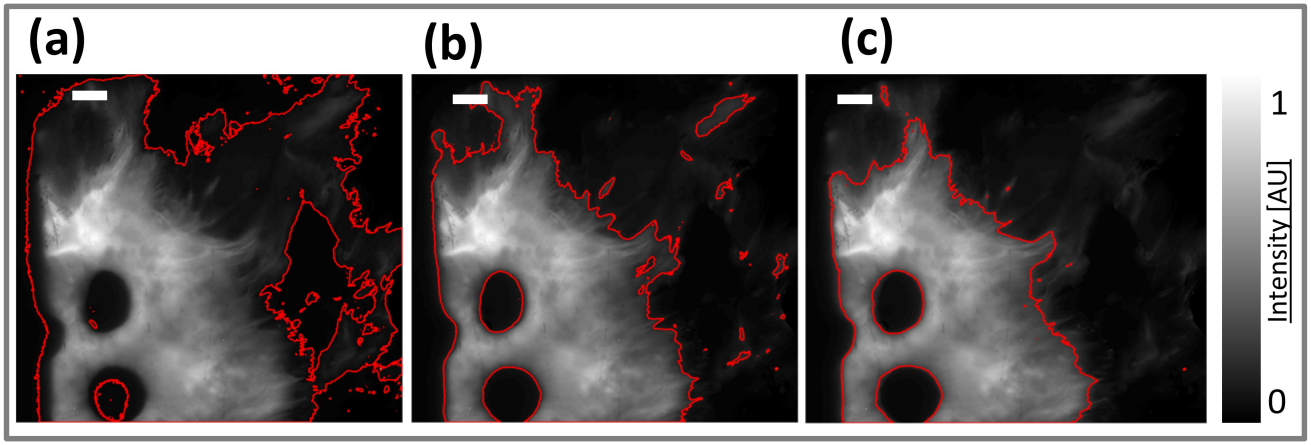
(a)
(b)
(c)
1
Intensity [AU]
0

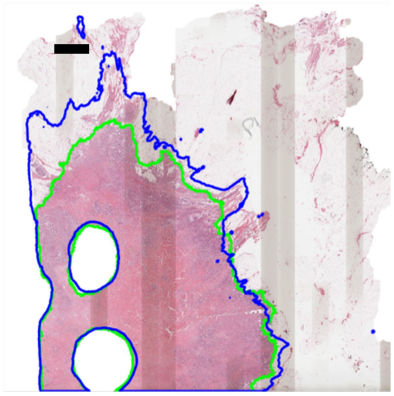
(d)

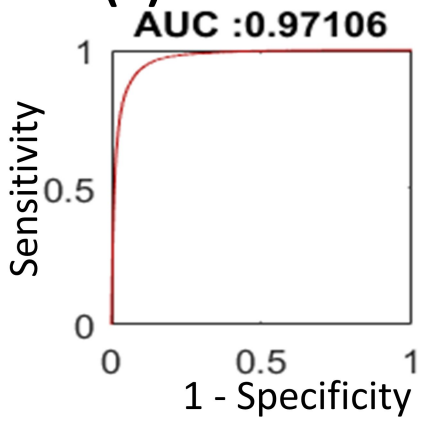
(e)
AUC :0.97106
Sensitivity
1
0.5
0
0
0.5
1
1 - Specificity

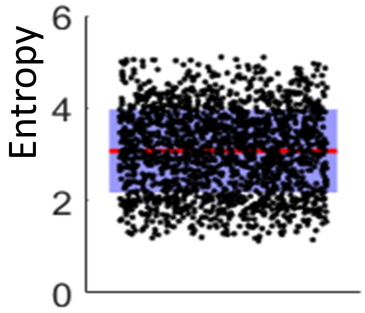
(f)
Entropy
6
4
2
0

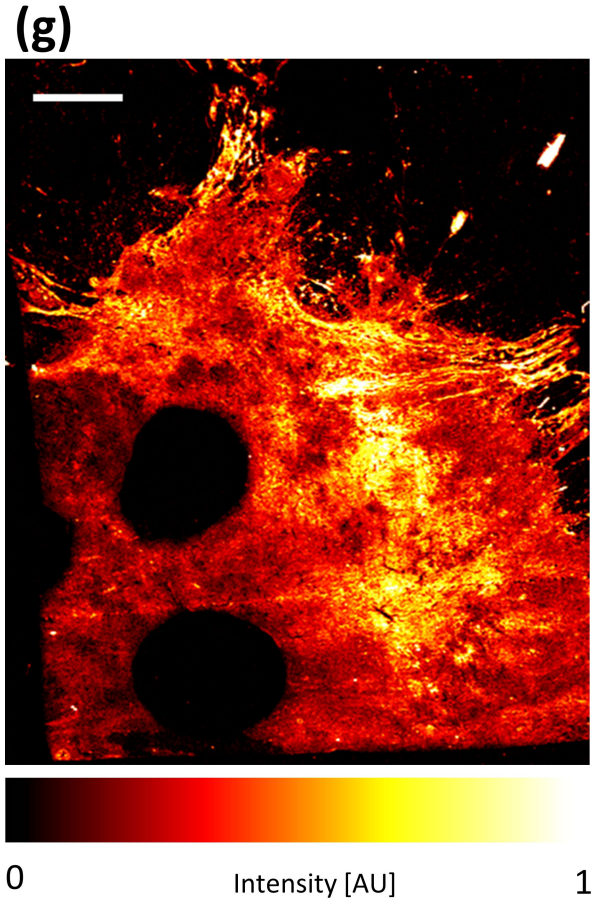
(g)
0
Intensity [AU]
1